Separation Science and Technology
Publication details, including instructions for authors and subscription information:
http://www.informaworld.com/smpp/title~content=t713708471

Heterogeneous Adsorption Characteristics of Volatile Organic Compounds (VOCs) on MCM-48

W. G. Shim[a]; J. W. Lee[b]; H. Moon[ac]
[a] Faculty of Applied Chemical Engineering, Chonnam National University, Gwangju, Korea [b] Department of Environmental and Chemical Engineering, Seonam University, Namwon, Korea [c] BK21 Center for Functional Nano Fine Chemicals, Chonnam National University, Gwangju, Korea

To cite this Article Shim, W. G. , Lee, J. W. and Moon, H.(2006) 'Heterogeneous Adsorption Characteristics of Volatile Organic Compounds (VOCs) on MCM-48', Separation Science and Technology, 41: 16, 3693 — 3719
To link to this Article: DOI: 10.1080/01496390600956936
URL: http://dx.doi.org/10.1080/01496390600956936

Separation Science and Technology, 41: 3693–3719, 2006

ISSN 0149-6395 print/1520-5754 online
DOI: 10.1080/01496390600956936

Heterogeneous Adsorption Characteristics of Volatile Organic Compounds (VOCs) on MCM-48

W. G. Shim
Faculty of Applied Chemical Engineering, Chonnam National University, Gwangju, Korea

J. W. Lee
Department of Environmental and Chemical Engineering, Seonam University, Namwon, Korea

H. Moon
Faculty of Applied Chemical Engineering, Chonnam National University, Gwangju, Korea and BK21 Center for Functional Nano Fine Chemicals, Chonnam National University, Gwangju, Korea

Abstract: This work focuses on the fundamental studies of heterogeneous adsorption characteristics of mesoporous adsorbent. MCM-48 was synthesized to investigate the adsorption properties of eight different volatile organic compounds (benzene, cyclohexane, n-hexane, toluene, methanol, acetone, methyl ethyl ketone (MEK), and trichloroethylene (TCE)). The gravimetric method was used to measure the adsorption equilibrium amount. Several simple and reliable methods such as isosteric enthalpy of adsorption, thermodynamic properties, condensation pressure, organophilicity, and adsorption energy distribution were evaluated to understand the surface heterogeneity of the VOCs + MCM-48 adsorption system. This work shows that the

Received 21 February 2006, Accepted 9 July 2006
W. G. Shim and J. W. Lee contributed equally to this work.
Address correspondence to H. Moon, Faculty of Applied Chemical Engineering, Chonnam National University, Gwangju 500-757, Korea. Tel.: + 82-62-530-1877; Fax: +82-62-530-1899; E-mail: hmoon@chonnam.ac.kr

unique features of the VOCs + MCM-48 adsorption system are highly dependent on the adsorption step, ionization potential, and Debye dipole moment of VOCs.

Keywords: Adsorption, adsorption energy distribution, isotherm, MCM-48, VOCs

INTRODUCTION

In general many adsorbents have not only well developed porous structures but also different types of pores (1). The ordered mesoporous silicates and aluminosilicates denoted as M41S have been the subject of much interest since they were first described by the Mobil Oil scientists in 1992 (2). These materials opened new possibilities in the field of sensor, chromatographic packing material, catalytic support, immobilized medium, template of advanced nano-materials, adsorption, and catalysis. Therefore, it led to an increasingly growing number of research in the synthesis, application, and characterization of these novel materials. The synthesis and utilization of these materials have been investigated by many researchers because of their peculiar characteristics such as large internal surface area, uniformity of pore size, easily controlled pore size, and high thermal stability (3–12).

The mesoporous silicates, M41S, are classified into several members including MCM-41, MCM-48, MCM-50, and other species. MCM-41 has a hexagonal (or cylindrical) array of unidirectional pores while MCM-48 has a highly ordered bicontinuous cubic (*Ia3d*) pore system. It has been reported that the structure of MCM-48 can be explained by the gyroid or G-surface which contains three-dimensional channel networks. The synthesis of M41S materials can be obtained using hydrothermal reactions of silicate anion in the presence of various surfactants. Unlike the synthesis of conventional molecular sieves, the ordered mesoporous materials were synthesized by using the liquid crystal templating mechanism. Depending on the class of surfactants that were used as crystal template and the synthesis conditions, it was possible to adjust the pore size to between 1.6 and 10 nm. Mesoporous materials, regardless of their structure, type and composition, usually have a plenty of silanol groups on mesopores because of their amorphous surface structure, indicating a highly hydrophilic surface (2, 3, 5–8, 15–19).

A considerable number of studies have been conducted on the adsorption characteristics and properties of various gases and organic vapors on mesoporous media. It can be classified into three main groups: common gases, water and organic compounds (6, 8, 10, 13, 14, 20–28). To date, most research have mainly been limited to the MCM-41 material having a uniform one-dimensional pore network, focusing on the adsorption properties at a single temperature and pore size system. However, some studies have been carried out on the effect of temperature, mechanical stability and pore size. Boger et al. (29) have

investigated the influence of the temperature, mechanical stability, and aluminum content on the adsorption characteristics of MCM-41. Zhao et al. (10), Choudhary and Mantri (27) and Rathousky et al. (30) have also reported on the influence of temperature on the adsorption of various volatile organic compounds (VOCs) on MCM-41. In practical applications, the mechanical stability is an important characteristic of an adsorbent (8, 29, 31, 32). The mechanical stability of silica mesoporous material such as MCM-41, MCM-48, and SBA-15 have been studied extensively using nitrogen adsorption, X-ray diffraction, NMR, and various organic vapors. Beck et al. (2), Nguyen et al. (26) and Qiao et al. (33) have studied adsorption equilibrium isotherm data on the different pore size mesoporous samples. Recently Lee et al. (13) and Oh et al. (14) have reported the adsorption of chlorinated volatile organic compounds (CVOCs), VOCs, and water vapor on various mesoporous adsorbents (MCM-41, MCM-48, SBA-1, SBA-15, and KIT-1) at different temperatures.

An understanding of the characteristics of adsorbents is crucial in designing, modeling, and optimizing the real adsorption-based application systems. However, there seems to be no systematic investigation on the adsorption equilibrium isotherms and thermodynamic features for the adsorption of organic molecules on MCM-48. Although it has great possibilities for many applications owing to their unique pore network system, little has been studied on the adsorption properties of nitrogen and organic vapors compared to that of MCM-41. Therefore, in this study, several useful methods such as isosteric enthalpy of adsorption, Gibbs free energy, condensation pressure, organophilicity, and adsorption energy distribution have been employed to obtain useful information on the adsorption of non-polar and polar molecules on the manufactured MCM-48 adsorbent.

EXPERIMENTAL

Materials Preparation and Reagents

To synthesize the MCM-48 mesoporous adsorbent, cethyltrimethylammonium bromide (CTMABr, $C_{19}H_{42}BrN$, Aldrich) and Ludox AS-40 (Du Pont, 40 mass% colloidal silica in water) were used as the template and the silicon source, respectively. The template was removed by calcinations at 873 K for 10 h at a heating rate of 1 K/min in air. A detailed procedure of the synthesis of MCM-48 adsorbents was described elsewhere (13, 14). The purity and the manufacturer of each adsorbates are as follows: benzene, 99.5% (Junsei Chemical Co.); toluene, 99.5% (Junsei Chemical Co.); n-hexane, 95.0% (Junsei Chemical Co.); cyclo-hexane, 99.5% (Kanto Chemical Co.); acetone, 99.5% (Yakuri Pure Chemical Co.); methanol, 99.9% (Carlo ERBA Reagent); methyl ethyl ketone (MEK), 97.0% (Yakuri Pure Chemical Co.); trichloroethylene (TCE), 99.5% (Junsei Chemical Co.). All chemicals were used as received without further treatment.

To confirm that the synthesized materials are proper for a given purpose, one should know the specific characteristics of adsorbents. Thus, the quality of MCM-48 prepared in this study was examined by X-ray diffraction (XRD) and nitrogen adsorption and desorption techniques. XRD data of MCM-48 were collected on a Phillips PW3123 diffractometer equipped with a graphite monochrometer and Cu K_α radiation of wavelength 0.154 nm wavelength. XRD patterns were obtained between 2° and 50° with a scan speed of 1°/min. Nitrogen adsorption and desorption isotherms, BET (Brunauer, Emmett, and Teller) surface areas (34), and BJH (Barrett, Joyner, and Halenda) method (35) for the synthesized adsorbents were measured at 77 K using a Micromeritics ASAP 2010 automatic analyzer.

Gravimetric Apparatus

The adsorption amount of VOCs vapor was measured by a quartz spring balance, which was placed in a closed glass system. An adsorbent sample of 0.1 g was placed on a quartz basket, which was attached to the end of a quartz spring (13, 36, 37). The MCM-48 adsorbents were vacuumed for 15 hours at 10^{-3} Pa and 250°C to remove the volatile impurities. A turbo molecular pump (Edward type EXT70) in combination with a rotary vacuum pump (Edward model RV5) was used to evacuate the system. Pirani and penning vacuum gauges (Edwards Series 1000) were used for the measurement of vacuum. The pressure of the system was measured using a Baratron absolute pressure transducer (MKS Instruments Type 127) and a power supply read-out instrument (Type PDR-C-1C). The variation of weight was measured using a digital voltmeter that was connected to the spring sensor. Equilibrium experiments on the selected organic molecules were carried out at 303.15 K, 313.15 K and 323.15 K.

RESULTS AND DISCUSSION

Adsorption Equilibrium Isotherm

The important physical properties and the unique feature of the synthesized MCM-48 such as XRD pattern, BET surface area, BJH average pore diameter, and pore volume have been reported in our previous studies (13, 14, 37). The obtained data were in good agreement with early addressing of other research groups. As mentioned previously, the adsorption equilibrium amount of seven organic molecules on manufactured MCM-48 were obtained by using the gravimetric technique at different temperatures. Figure 1 shows the representative adsorption equilibrium isotherms of seven different VOCs on MCM-48 at 303.15 K in terms of concentration. It was found that the measured adsorption isotherm data shows the type

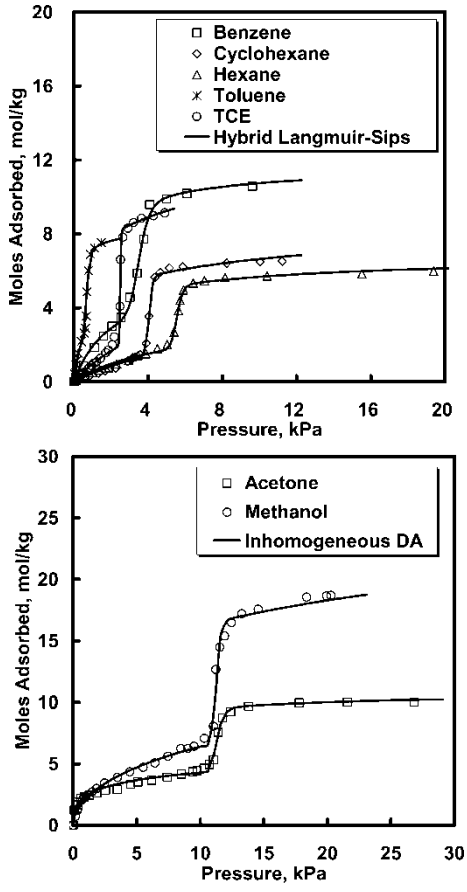

Figure 1. Representative adsorption isotherms of seven different VOCs on MCM-48 at 303.15 K.

IV, which represents the surface adsorption in the low pressure region and the capillary condensation at moderate pressure caused by the mesoporous characteristics of MCM-48. Also, MCM-48 have a narrow pore size distribution and capillary condensation can be observed at $P/P_0 = 0.2$ to 0.3. It has a higher affinity to polar organic adsorbates than to non-polar organics. As can be seen from this figure, the adopted hybrid isotherm model (Langmuir + Sips) and the inhomogeneous Dubinin-Astakov (DA) equation successfully correlated the adsorption equilibrium isotherm data although they do not have any physical meaning. The adsorption equilibrium isotherm models used are summarized in Table 1. The adsorption equilibrium data and estimated adsorption isotherm parameters have been presented in our previous results (13, 38). Especially, the hybrid isotherm described the non-polar organic compounds well, and the inhomogeneous

Table 1. Pure component adsorption isotherms used in this work

Model equations	
Hybrid Langmuir–Sips	
$N = m\left[\left(\frac{b_1 P}{1+b_1 P}\right)+\left(\frac{b_2 P^n}{1+b_2 P^n}\right)\right]$	$m = m_0 \exp\left(\frac{\alpha}{R}\left(\frac{1}{T}-\frac{1}{T_m}\right)\right)$
	$b_1 = b_{10} \exp\left(-\frac{\Delta H_1}{R}\left(\frac{1}{T}-\frac{1}{T_m}\right)\right)$
	$b_2 = b_{20} \exp\left(-\frac{\Delta H_2}{R}\left(\frac{1}{T}-\frac{1}{T_m}\right)\right)$
	$n = n_0 \exp\left(-\frac{\delta}{R}\left(\frac{1}{T}-\frac{1}{T_m}\right)\right)$
Parameters	m_0, α, b_{10}, ΔH_1, b_{20}, ΔH_2, n_0, δ
	T_m = mean temperature
Inhomogeneous DA	
$N = W\left[\exp\left(-\frac{A}{\beta \cdot E_{01}}\right)^{n1}+\exp\left(-\frac{A}{\beta \cdot E_{02}}\right)^{n2}\right]$	$A = RT \cdot \ln\left(\frac{P_0}{P}\right)$
	$\beta = \frac{V_m}{V_m^{\mathrm{ref}}}(V_m^{ref} = \text{benzene})$
	$W = W_0 \exp[-\gamma (T - T_m)]$
Parameters	W_0, γ, E_{01}, E_{02}, $n1$, $n2$
	T_m = mean temperature

DA model was useful in explaining the adsorption isotherm data of polar VOCs (13, 14, 37, 38).

Isosteric Enthalpy of Adsorption

As a useful thermodynamic property, the isosteric enthalpy of adsorption has been generally applied to characterize the adsorbent surface (39, 40) The isosteric enthalpy is a measure of the interaction between adsorbate molecules and adsorbent lattice atoms, and it may be used as a measure of the energetic heterogeneity of a solid surface. It has been recognized that surface heterogeneity may come from the energetic, structural, and geometric heterogeneity. For a heterogeneous adsorption system, the isosteric enthalpy curve varies with the surface loading. Information concerning the magnitude of the enthalpy of adsorption and its variation with coverage can provide useful information about the nature of the surface and the adsorbate phase. It is generally known that the adsorption is accompanied by evolution of heat since adsorbate molecules are more stabilized on the adsorbent surface than in the bulk phase. The isosteric enthalpy of adsorption (q_{st}) can be calculated by the Clausius-Clapeyron equation.

An adsorption isotherm model should be expressed as a function of temperature to determine the isosteric enthalpy of adsorption from adsorption

isotherm. The equation, when integrated, allows one to calculate q_{st} from adsorption isotherms obtained experimentally at three temperatures, provided that the range of temperatures is small enough to justify the assumption that q_{st} is independent of temperature.

$$(\ln p)_N = -\frac{q_{st}}{RT} \tag{1}$$

where p is the pressure, T is the temperature, and R is the gas constant.

Based on the above approach, the isosteric heat curves of the proposed hybrid isotherms can be calculated as follows:

For the Hybrid Langmuir-Sips isotherm

$$q_{st} = \frac{\{\alpha(b_1P)(1+b_1P) + (-\Delta H_1)(b_1P)\}(1+b_2P^n)^2}{b_1P(1+b_2P^n)^2 + b_2nP^n(1+b_1P)^2} + \frac{\begin{array}{c}\{\alpha(b_2P^n)(1+b_2P^n) + (-\Delta H_2)(b_2P^n) + n(b_2P^n) \\ \times \ln P(-\delta)\}(1+b_1P)^2\end{array}}{b_1P(1+b_2P^n)^2 + b_2nP^n(1+b_1P)^2} \tag{2}$$

where, b_1, b_2, n, ΔH_1, ΔH_2, α, δ are the hybrid isotherm parameters (Table 1).

For the inhomogeneous DA isotherm

$$q_{st} = \frac{\gamma \cdot T \cdot [\exp(-A/\beta \cdot E_{01})^{n1} + \exp(-A/\beta \cdot E_{02})^{n2}]}{\begin{array}{l}[n1 \cdot A^{n1-1}/(\beta \cdot E_{01})^{n1} \cdot \exp(-A/\beta \cdot E_{01})^{n1} \\ +n2 \cdot A^{n2-1}/(\beta \cdot E_{02})^{n2} \cdot \exp(-A/\beta \cdot E_{02})^{n2}]\end{array}} + (A + \Delta H_{vap}) \tag{3}$$

where, A is the adsorption potential, ΔH_{vap} is the heat of vaporization, β is the affinity coefficient, and n_1, n_2, E_{01}, E_{02} are the inhomogeneous DA isotherm parameters (Table 1).

Figure 2 shows the comparisons of isosteric heat curves by the hybrid Langmuir-Sips and inhomogeneous models for cyclohexane. As can be seen in Fig. 2, the variation of the heat curve calculated by the hybrid Langmuir-Sips equation is quite complex. The heat of adsorption is consistent under 0.95 mol kg^{-1} and over about 5.7 mol kg^{-1} of adsorbed amount. However, the heat curve obtained by this isotherm equation is sharply decreased at the intermediated adsorbate loading, ranging from 0.95 to 5.7 mol kg^{-1}. The shape of the heat curve resembles the concave surface. In addition, the result of the heat curve by the inhomogeneous DA equation gives improper quantities at the limit of zero and maximum loading because of the thermodynamic inconsistency.

The sharp variation of enthalpy of adsorption for the various VOCs with surface coverage shown in Fig. 3 supports that bonding among VOC molecules in the condensed phase and between the adsorbed VOCs layer and the MCM-48 surfaces play a key role in determining the desorption characteristics. In addition, the isosteric enthalpy of adsorption is considered to be the isosteric enthalpy of desorption. MCM-48 surface seems to be

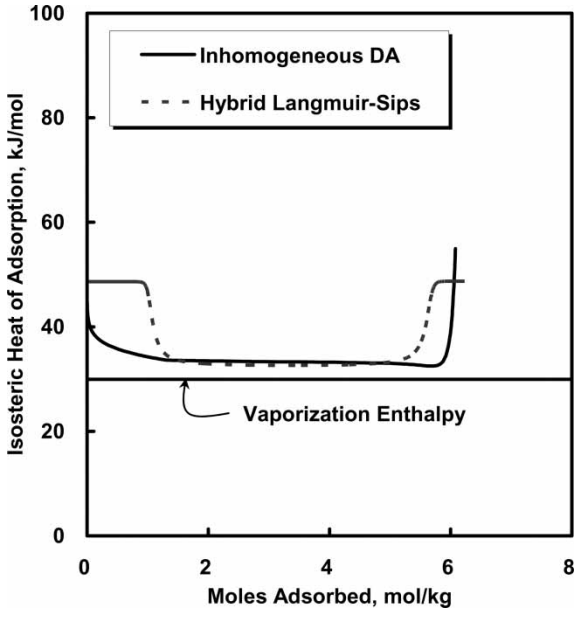

Figure 2. Comparison of isosteric heat of adsorption of cyclohexane between Hybrid Langmuir-Sips and Inhomogeneous DA equations. [Hybrid Langmuir-Sips parameters: $m_0 = 4.242$, $\alpha = 1.905 \times 10^{1}$, $b_{10} = 6.430 \times 10^{-2}$, $\Delta H_1 = -4.861 \times 10^{4}$, $b_{20} = 5.244 \times 10^{-21}$, $\Delta H_2 = -8.258 \times 10^{5}$, $n_0 = 2.547 \times 10^{1}$, $\delta = 1.821 \times 10^{2}$; Inhomogeneous DA parameters: $W_0 = 3.616$, $\gamma = 1.991 \times 10^{-6}$, $E_{01} = 2.817 \times 10^{3}$, $E_{02} = 2.977 \times 10^{3}$, $n1 = 2.113 \times 10^{1}$, $n2 = 1.431$]

heterogeneous because the isosteric enthalpy of adsorption changes according to the loading as shown in Fig. 3 (10, 53–55). These results are classified into three sections:

1. Decreased (or increased) with an increasing adsorbed amount in the range of surface adsorption.
2. Approaching a constant value related with the capillary condensation.
3. Increased (or decreased) with an increasing adsorbed amount in the range of exterior adsorption.

Table 2 summarizes the results of isosteric enthalpy of adsorption and ionization potential for different VOCs. Previous studies have shown that the isosteric enthalpy of adsorption of VOCs is related with the ionization potential of organic compounds. The isosteric enthalpy of adsorption decreased with an increase in ionization potential. The results of this study are in agreement with the reports of other researchers (27). The order of magnitude for the average isosteric enthalpy of adsorption and ionization potential of VOCs is as follows

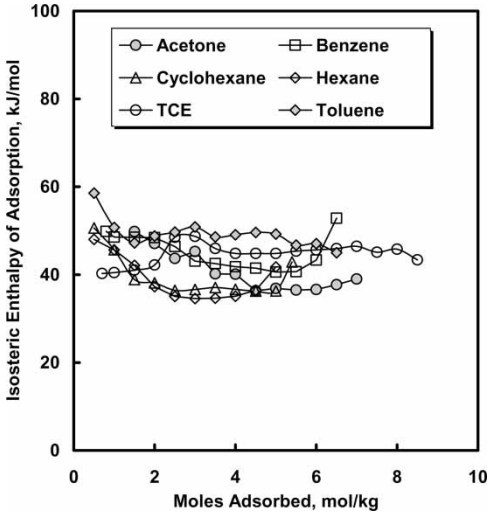

Figure 3. Isosteric enthalpy of adsorption of six organic vapors.

- Average isosteric enthalpy of Adsorption: Toluene > Benzene > TCE > Acetone > Cyclohexane > n-Hexane
- Ionization potential of VOCs: n-Hexane > Cyclohexane > Acetone > TCE > Benzene > Toluene

In the light of these results, it is appropriate to note that the variations of isosteric enthalpy of adsorption for organic molecules with surface coverage are highly associated with the energetic heterogeneity of MCM-48 surface.

Table 2. The average isosteric enthalpy of adsorption, molecular weight, Debye dipole moment and ionization potential of VOCs

Adsorbate	ΔH (kJ mol^{-1})	Molecular weight	Debye dipole moment	Ionization potential (eV)
Benzene	45.24	78.11	0.0	9.25
Cyclohexane	39.59	84.16	0.3	9.86
n-Hexane	39.07	86.18	0.0	10.13
Toluene	48.90	92.14	0.4	8.82
Methanol	ND	32.04	1.7	10.85
Acetone	40.77	58.08	2.9	9.71
TCE-powder	44.67	131.39	0.9	9.47

(ND: Not determined).

Gibbs Free Energy and Entropy Changes in Adsorption

In order to examine the thermodynamic properties for adsorption of VOCs on MCM-48 at different temperatures, the following equations were used;

$$\Delta G = -RT \ln\left(\frac{P_{\text{standard}}}{p}\right) \tag{4}$$

$$\Delta S = \frac{\Delta H - \Delta G}{T} \tag{5}$$

where, ΔG is the Gibbs free energy, P_{standard} is the standard pressure, R is the gas constant, T is the temperature, ΔH is the enthalpy of adsorption, and ΔS is the entropy of adsorption. Using these definitions, the thermodynamic characteristics of benzene at different temperatures are obtained and listed in Table 3. With increasing temperatures and an increasing adsorbed amount, the Gibbs free energy ($-\Delta G$) decreases and also the entropy of adsorption ($-\Delta S$) varies greatly.

It is also possible to obtain the changes of entropy in the adsorption at different temperatures as follows (27):

$$S_{t3D} = R \ln((MW)^{1.5}(T)^{2.5}) - 9.61 \tag{6}$$

$$S_{t2D} = 0.066 \cdot S_{t3D} + 2.76 \ln(T) - 12.71 \tag{7}$$

$$\Delta S_m = \Delta S + R \ln\left(\frac{A^*_{m\,\text{standard}}}{A_m}\right) \tag{8}$$

$$A^*_{m\,\text{standard}} = 4.08T \times 10^{-16}\ \text{cm}^2 \tag{9}$$

where S_{t3D} is the translational entropy of three dimensions, MW is the molecular weight, S_{t2D} is the translational entropy of two dimensions, ΔS_m is the observed entropy change, $A^*_{m\,\text{standard}}$ is the standard molecular area, and A_m is the adsorbate molecular area. In the case of no loss of rotational degrees of freedom of adsorbed molecules, the values of the entropy of mobile and localized adsorption are $S_{t3D} - S_{t2D}$ and S_{t3D}. Table 4 summarizes the obtained values of the entropy change, that is, S_{t3D}, S_{t2D} and $S_{t3D} - S_{t2D}$ for the different VOCs at 303.15 K. The values of the mobile and localized adsorption entropy obtained are in the ranges of 47–53J $\text{K}^{-1}\,\text{mol}^{-1}$ and 152–170J $\text{K}^{-1}\,\text{mol}^{-1}$, respectively. Figure 4 indicates that the changes of the observed entropy depend greatly on the adsorbed amount. These results are similar to that of isosteric enthalpy of adsorption. It can be divided into three parts: surface adsorption, capillary condensation, and exterior adsorption. In other words, as the adsorbed amount increases, the observed entropies

1. decreases (or increases),
2. reaches a constant value and then
3. increases (or decreases).

Table 3. Thermodynamic data for adsorption of benzene

Adsorbed Amount	303.15 K			313.15 K			323.15 K		
	$-\Delta G$ (kJ/mol^{-1})	$-\Delta S$ (J mol^{-1})	$-\Delta S_m$ (J mol^{-1})	$-\Delta G$ (kJ/mol^{-1})	$-\Delta S$ (J mol^{-1})	$-\Delta S_m$ (J mol^{-1})	$-\Delta G$ (kJ/mol^{-1})	$-\Delta S$ (J mol^{-1})	$-\Delta S_m$ (J mol^{-1})
0.80	13.017	122.713	94.162	10.529	126.369	97.519	10.722	121.457	92.318
1.00	12.243	121.029	92.478	10.028	123.869	95.018	9.969	119.820	90.681
1.50	10.988	125.085	96.534	8.820	127.631	98.781	8.623	123.883	94.744
2.00	9.923	128.336	99.785	7.873	130.387	101.537	7.483	121.147	98.008
2.50	8.929	124.951	96.400	7.046	126.585	97.735	6.545	123.818	94.679
3.00	8.471	115.369	86.818	6.787	116.702	87.852	6.720	114.322	85.183
3.50	8.399	113.724	85.173	6.752	114.995	86.145	6.229	112.691	83.552
4.00	8.328	111.484	82.933	6.718	112.720	83.869	6.202	110.470	81.331
4.50	8.260	110.632	82.081	6.701	111.732	82.882	6.149	109.628	80.489
5.00	8.193	107.909	79.358	6.650	109.054	80.204	6.136	106.925	77.786
5.50	8.161	108.267	79.716	6.568	109.559	80.709	6.097	107.279	78.139
6.00	8.129	117.324	88.773	6.411	118.696	89.846	5.887	116.270	87.131
6.50	7.914	149.788	121.237	5.939	150.839	121.989	5.029	148.516	119.377

Table 4. The translational entropy values of VOCs at 303.15 K

Adsorbate	S_{t3D}	S_{t2D}	$S_{t3D}-S_{t2D}$
Benzene	163.29	111.95	51.34
Cyclohexane	164.22	112.57	51.65
n-Hexane	164.52	112.77	51.75
Toluene	165.35	113.32	52.03
Methanol	152.18	104.54	47.64
Acetone	159.60	109.48	50.11
TCE	169.78	116.27	53.50

Except for the adsorption of TCE (powder) and toluene, the observed entropy change approaches the mobile adsorption in the range of capillary condensation. It needs to be noted that these obtained values with the theoretical method are in between mobile and localized adsorption. On the whole, however, it seems to be closer to the mobile adsorption than to the localized adsorption.

Condensation Pressure

If one can predict the condensation pressure, a higher working capacity can be achieved by controlling the pore size of mesoporous adsorbents. It has been known that the condensation pressure depends on the adsorbate, temperature, pore size, and geometry of the adsorbent. In general the Kelvin equation has been widely used for the adsorption of nitrogen on mesoporous media to calculate the condensation pressure as a function of temperature. However, in this study the Broekhoff and the de Boer equation were used to obtain it. The main difference between the two equations is the thermodynamic potential of the adsorbed layer. Recently, Qiao et al. (33) used this equation to explain the nitrogen adsorption isotherms for mesoporous adsorbents of different pore size. Rearranging the Broekhoff and de Boer equations gives

$$P_c = P_0 \cdot \exp\left[\frac{2 \cdot \sigma \cdot V_m \cdot \cos\theta}{r_P - t} \cdot \frac{1}{R \cdot T}\right] - F(t) \qquad (10)$$

where P_c is the capillary condensation pressure, P_0 is the vapor pressure, σ is the liquid surface tension, V_m is the molar volume of the condensed adsorbate, θ is the contact angle between the solid and condensed phase (taken to be zero here, thus $\cos\theta = 1$), r is a pore radius (here 1.6 nm for MCM-48), and r_P is the molecular radius of adsorbate, and $F(t)$ is the thermodynamic potential of the adsorbed layer. Since both the molar volume and the surface tension are temperature-dependent properties,

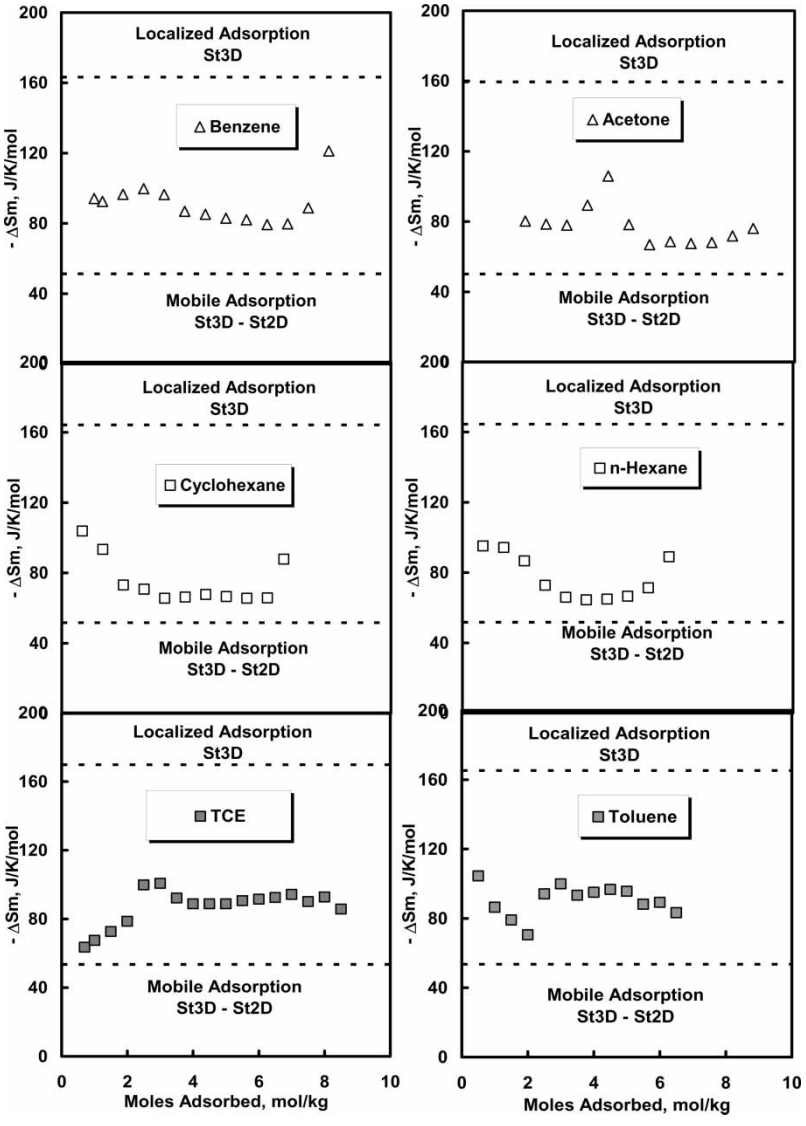

Figure 4. Observed entropy changes of benzene, acetone, cyclohexane, n-hexane, TCE, and toluene.

Gunn and Yamada correlation and values given in literature (Reid et al. (41)) were used.

In order to determine the condensation pressure, the proposed hybrid isotherms were used. As discussed in our previous report (37), the hybrid isotherms have the unique feature that Langmuir (or DA-1) isotherms describes the surface adsorption part at low pressure while Sips (or DA-2)

isotherms explains the capillary condensation regions at moderate pressure. Therefore, the distinct point between two regions can be obtained using the hybrid isotherms. Here we assumed that the obtained points from the model equations correspond to the condensation pressure. Based on these methods, the thermodynamic potentials of the adsorbed layer were determined, and they are summarized in Table 5. These results can be classified into two main groups. When the Debye dipole moments are lower than 0.50, the thermodynamic potentials of the adsorbed layer have a certain amount, except for the cases of methanol. However, in the case of adsorbates that have high Debye dipole constant (>0.5), there is no need for thermodynamic values to match the point of condensation pressure. Consequently, the Debye dipole moments are expected to be related to the thermodynamic potentials of the adsorbed layer.

Organophilicity of MCM-48

The thermal gravimetric (TG) desorption method is useful in investigating the physical adsorption, pore configuration, and the relationship between the adsorbate-adsorbate. In this study, desorption of VOCs on MCM-48 was conducted at a heating rate of 10 K min^{-1} using the quartz spring balance. Figure 5 shows (top) the weight loss curves and (bottom) the differential TG profiles of benzene, methanol, hexane, cyclo-hexane, acetone, and toluene on MCM-48. Previous studies have shown that the MCM-41 adsorbent which has a one dimensional and cylindrical pore network had only one peak desorption curves of different VOCs. Considering the regeneration of an adsorbent, this characteristic is very useful to understand and develop the solvent recovery process. At the initial stage, the non-polar adsorbates have lower gradients of weight loss and then it changes with increasing temperature. It was reported that the surface properties can be divided into two cases: organophilic and organophobic. This can be determined from the difference between the weight loss peak (T_d) and adsorbate boiling point (T_b). In other words the negative value means the surface is organophobic while the organophilic surface has the positive value. The results obtained from the above definitions are summarized in Table 6. It might be inferred from the affinity values of VOCs on MCM-48 that the surface is organophobic. The order of affinity to VOCs on MCM-48 is quite similar to that of reported data, that is, acetone $>$ methanol $>$ n-hexane $>$ benzene $>$ cyclo-hexane $>$ toluene. Therefore, it can be concluded that the adsorption affinity to MCM-48 is closely associated with the polarity of adsorbates.

Adsorption Energy Distribution

Adsorption phenomena onto porous solids is very complex because the structure of adsorbent is quite complex and also is not easy to define it

Table 5. Determined thermodynamic potential values of VOCs

Temperature K	Benzene	Toulene	n-Hexane	cyclo-Hexane	TCE	Methanol	Acetone
Thermodynamic potential of the adsorbed layer F(t)							
303.15	0.35	0.35	0.3	0.7	0.0	0.6	0.0
313.15	0.35	0.35	0.2	0.4	0.0	−0.5	0.0
323.15	0.35	0.35	0.1	0.3	0.0	ND	0.0

(ND: Not determined).

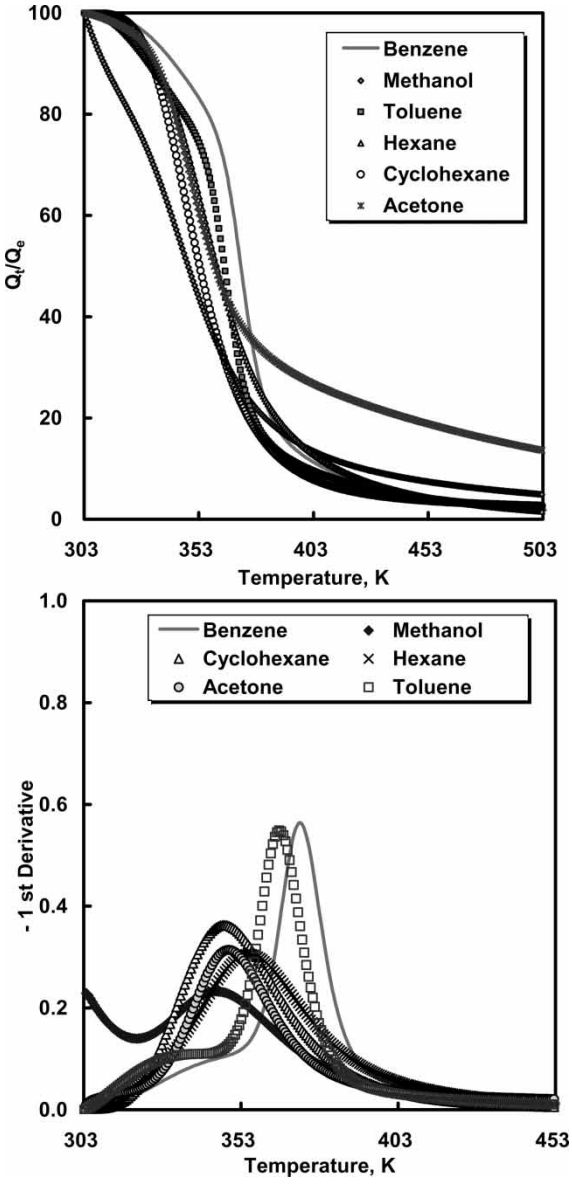

Figure 5. Thermal desorption curves and the differential curves of thermal desorption of VOCs on MCM-48 at a heating rate of 10 K/min.

(42, 43). Adsorption heterogeneity in general is associated with characteristics between the adsorbent and adsorbate.

The overall adsorption isotherm on the heterogeneous solid surface can be written in the form of

Table 6. Weight loss peak position and the affinity of MCM-48 to VOCs

Adsorbate	Weight loss peak, T_d/K (MCM-48)	Adsorbate boiling point, T_b/K	$T_d - T_b$/K (MCM-48)
Benzene	336.4	353.3	−16.8
Cyclohexane	324.8	353.9	−29.0
n-Hexane	328.4	342.2	−13.8
Toluene	340.2	383.8	−43.6
Methanol	333.2	337.8	−4.6
Acetone	325.5	329.4	−3.9

$$\theta(p) = \int_0^x \theta(p, x) \cdot F(x) \cdot dx \quad T = \text{constant} \tag{11}$$

where p is the equilibrium pressure, x is the adsorption pore size, energy and so on, $F(x)$ is the distribution function of the energetic and structural parameters, $\theta(p, x)$ is a local adsorption isotherm and $\theta(p)$ is the experimental adsorption isotherm data. This is called the Fredholm integral equation of the first kind. The calculation of this distribution function is the well known ill-posed problem. The main difficulties in solving the equation are

1. small variations in the experimental data may lead to large changes in the distribution function, and
2. a large set of possible solutions to this equation can produce a distorted result.

Therefore, a proper determination of the distribution function from the experimental adsorption data is of great importance for the characterization of heterogeneous adsorbents. In the last 30 years, many attempts have been made to get a meaningful solution with respect to the distribution function (42–45). In general, a proper solution of the integral equation can be obtained from the analytical methods, numerical methods, and local adsorption isotherm approximation methods. In this work, the program generalized nonlinear regularization method, which can avoid the difficulties caused by the ill-posed nature of an adsorption integral equation, was modified to solve the problem (46, 47). The local adsorption isotherms such as Langmuir, Volmer, Fowler Guggenheim, Hill-de Boer, and BET equations are used extensively in obtaining the proper adsorption energy distribution (48–51). Among the proposed equations, the Fowler Guggenheim isotherm, that describes the localized monolayer adsorption with lateral interaction, was used to describe the adsorption energy distribution for nitrogen.

The Fowler Guggenheim (FG) equation is as follows,

$$\theta(p, E) = \frac{K \cdot p \cdot \exp(zw\Theta/k_BT)}{1 + K \cdot p \cdot \exp(zw\Theta/k_BT)} \tag{12}$$

where T is the absolute temperature, p is the equilibrium pressure, z is the number of nearest neighbor molecules in the monolayer, w is the interaction energy between two nearest neighbor molecules, k_B is the Boltzmann constant, $K = K_0(T) \cdot \exp(E/k_BT)$ is the Langmuir constant, and the pre-exponential factor $K_0(T)$ can be calculated from the partition functions for an isolated molecule.

The BET equation was presented to explain the multilayer adsorption. Although the original BET equation is useful for describing the adsorption isotherm of Type I to Type III, it is not suitable to explain the Type IV and Type V equations. Therefore, Brunauer et al. (52) introduced a modified BET isotherm equation as follows,

$$\theta = \frac{V}{V_m} = \frac{C \cdot x}{1 - x} \times \frac{1 + (ng/2 - n)x^{n-1} - (ng + 1)x^n + ((ng/2) + (n/2))x^{n+1}}{1 + (C - 1)x + ((Cg/2) - (C/2))x^n - ((Cg/2) + (C/2))x^{n+1}} \tag{13}$$

$$C = \gamma \cdot \exp\left(\frac{E - Q_L}{RT}\right) \tag{14}$$

$$x = \frac{P}{P_0} \tag{15}$$

$$g = \exp\left(\frac{\Delta\varepsilon}{RT}\right) \tag{16}$$

$$\Delta\varepsilon = \frac{Q_L}{4} \quad \text{or} \quad \frac{E}{5} \tag{17}$$

where C is the BET constant, n is the number of adsorption layers, Q_L is the liquefaction heat, $\Delta\varepsilon$ is the excess of the evaporation heat.

In this work, a generalized nonlinear regularization method was adopted to investigate the adsorption energy distribution (46, 47). Before discussing the adsorption energy distribution in mesoporous adsorbents, it will be useful to verify this method for solving adsorption integral equations. Thus, simulated adsorption isotherms that have different energy distribution such as one, three, and five Gaussian peaks, were evaluated. The Langmuir adsorption equation was used to represent the local adsorption isotherm. Detailed information was collected from Brauer et al. (48). Figure 6 shows the theoretical adsorption isotherms and the postulated distribution functions with the energy distribution functions obtained from the above proposed procedure at the regularization parameter $\alpha = 1 \times 10^{-3}$. Except for the energy distribution function with five Gaussian peaks, the results are highly consistent with the

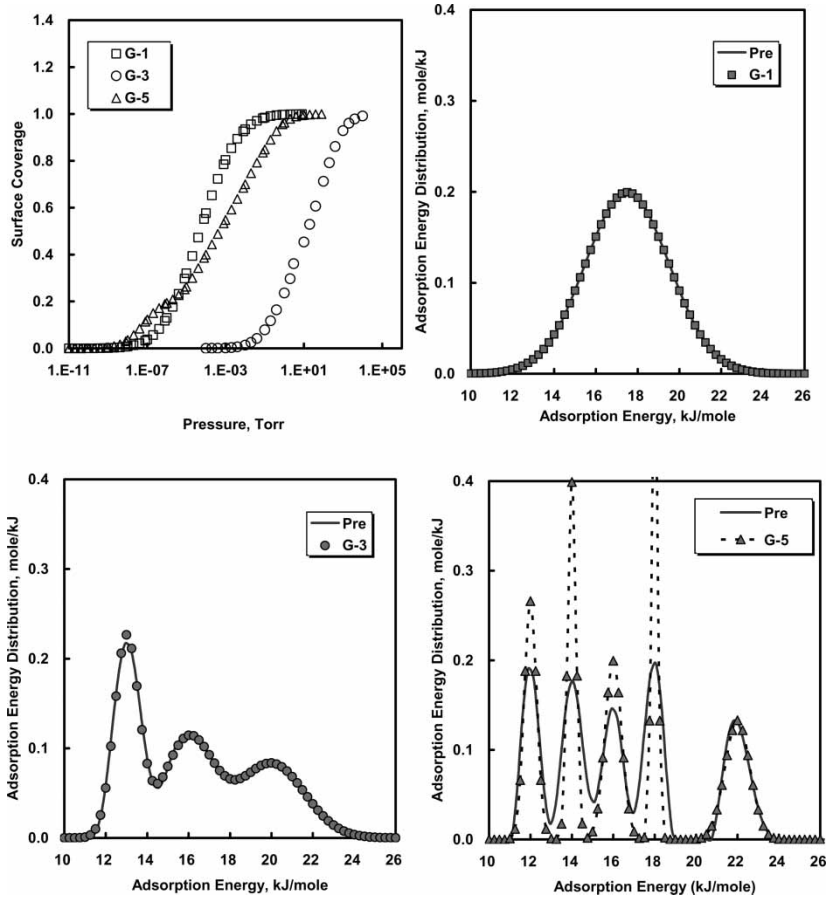

Figure 6. Simulated adsorption isotherms and comparison of postulated and calculated energy distributions.

simulated data. On the basis of the results of the test run, it is apparent that this approach is also useful to treat the adsorption surface heterogeneity such as INTEG (49), CONTIN (50), and other methods (42, 43, 45).

Recently, the adsorption energy distribution curves of mesoporous materials have been reported (19). For the comparison purpose, thus, we examine the applicability of the nonlinear regularization method used in this work to obtain the nitrogen adsorption energy distribution of MCM-48. The calculation procedure and parameters are addressed by Kruk et al. (19). Figure 7 shows the nitrogen adsorption energy distribution for MCM-48 adsorbent. It was obtained using the form of Fowler-Guggenheim localized equation. Also the interaction energy between the nearest molecules was set to be 190 K. Previous studies have shown that the interaction parameter

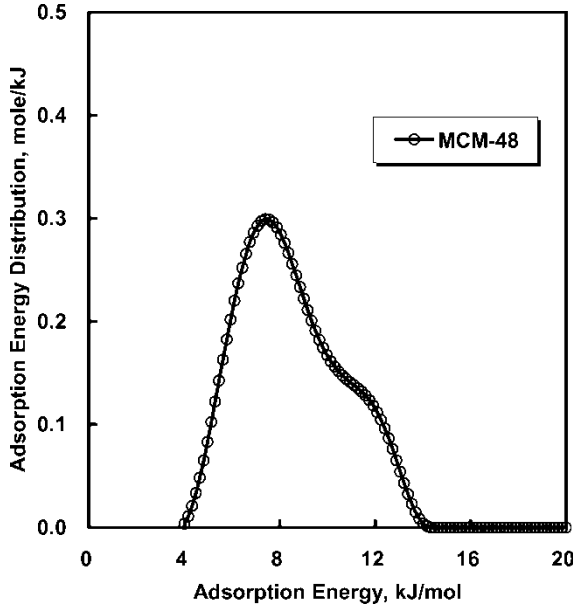

Figure 7. Nitrogen adsorption energy distribution calculated with the Fowler-Guggenheim equation.

affected the position of the peak while the regularization parameter that is related to the numerical stability of the solutions was sensitive to the adsorption energy distribution. The highest peak of adsorption energy distribution under this approach was found to be around 7.5 kJ mol^{-1}. It is interesting that the obtained curve in this study is similar to the reported adsorption energy distribution for mesoporous adsorbents (19). It was found from this result that the nonlinear regularization method can be successfully applied to obtain the adsorption energy distribution of mesoporous materials.

In order to investigate the adsorption energy distributions of VOCs, the modified BET model equation was chosen. In general, the adsorption isotherms of VOCs can be divided into three parts:

1. surface adsorption (Part 1),
2. capillary condensation (Part 2), and
3. exterior adsorption (Part 3).

In order to examine the trend of adsorption energy distribution, we used different conditions; these are the adsorption isotherms of the entire region (All) and separated parts (Part1, Part 2 and Part 3). Figures 8 and 9 show the representative results of adsorption energy distribution of benzene (non-polar) and acetone (polar) on MCM-48 at different temperatures. As shown

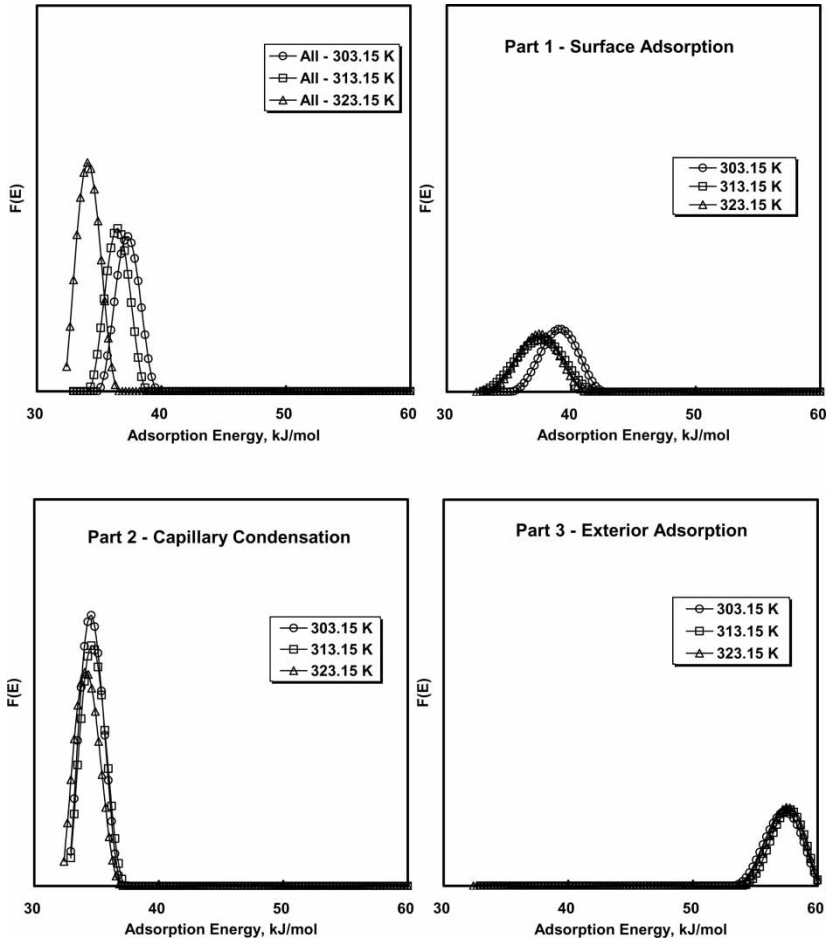

Figure 8. Benzene adsorption energy distributions calculated with the BET equation.

in Fig. 8, the pattern of adsorption energy distribution obtained in this work is directly related to the adsorption step. In the range of surface adsorption, the adsorption energy has a relatively high position (main peaks at about 32–42 kJ mol^{-1}) while it is close to the vaporization enthalpy in capillary condensation (main peaks at about 32–37 kJ mol^{-1}). Finally, the adsorption energy distribution patterns of the VOCs on MCM-48 moved into higher energy positions in the exterior adsorption part (main peaks at about 53–60 kJ mol^{-1}). When the whole adsorption isotherm data was used, the capillary condensation region dominated the adsorption energy except for the several adsorbates such as acetone (Fig. 9), methyl ethyl ketone, and methanol, which have a high Debye dipole constant. In other words, for polar molecules the energy distribution curves are also affected mainly by

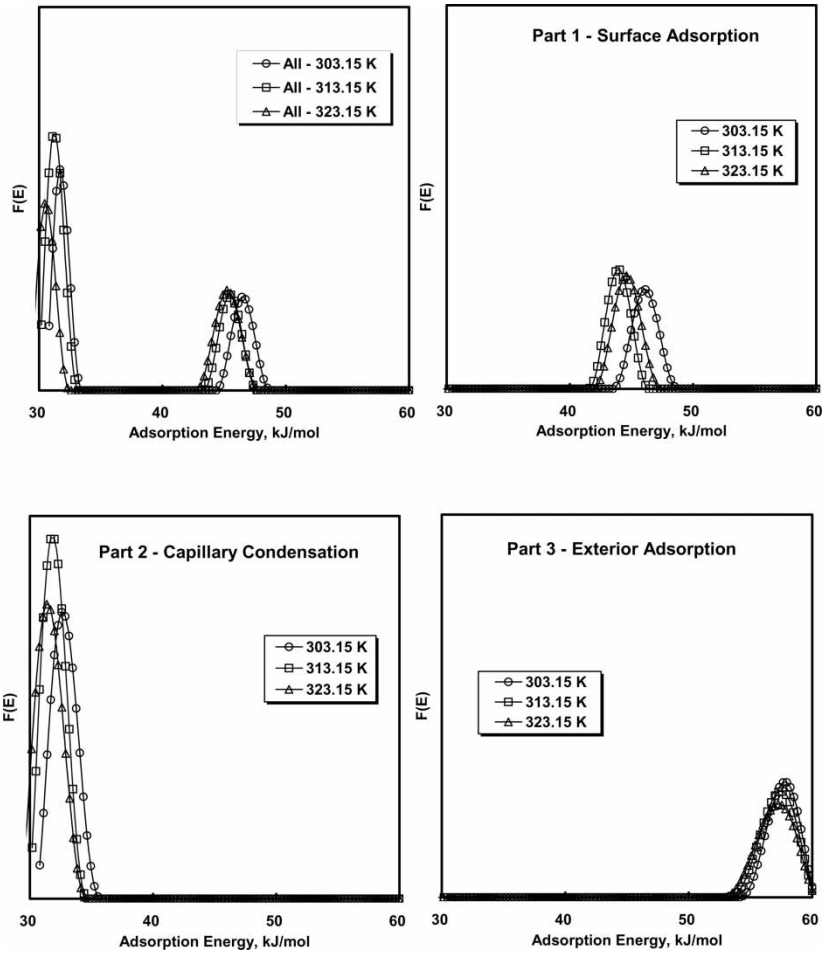

Figure 9. Acetone adsorption energy distributions calculated with the BET equation.

the surface adsorption region. Thus, one should consider the effect of surface adsorption as well as the capillary condensation to explain the system. Furthermore, the adsorption temperature influences the position of the adsorption energy peaks, especially in the capillary condensation region. In Fig. 10, the adsorption energy distribution curves for non-polar molecules have one peak on MCM-48, while the functions for polar adsorbates revealed two peaks. For example, the obtained high energy peak of acetone appears at 46.4 kJ mol^{-1}, and the maximum of low energy peak is located at about 31.7 kJ mol^{-1} and the intensity of the first peak is about two times higher than that of the second. However, the trend of the adsorption energy curve of methyl ethyl ketone is different from the results of acetone and methanol. In other words, the second peak appears between 47 and 52 kJ mol^{-1} and

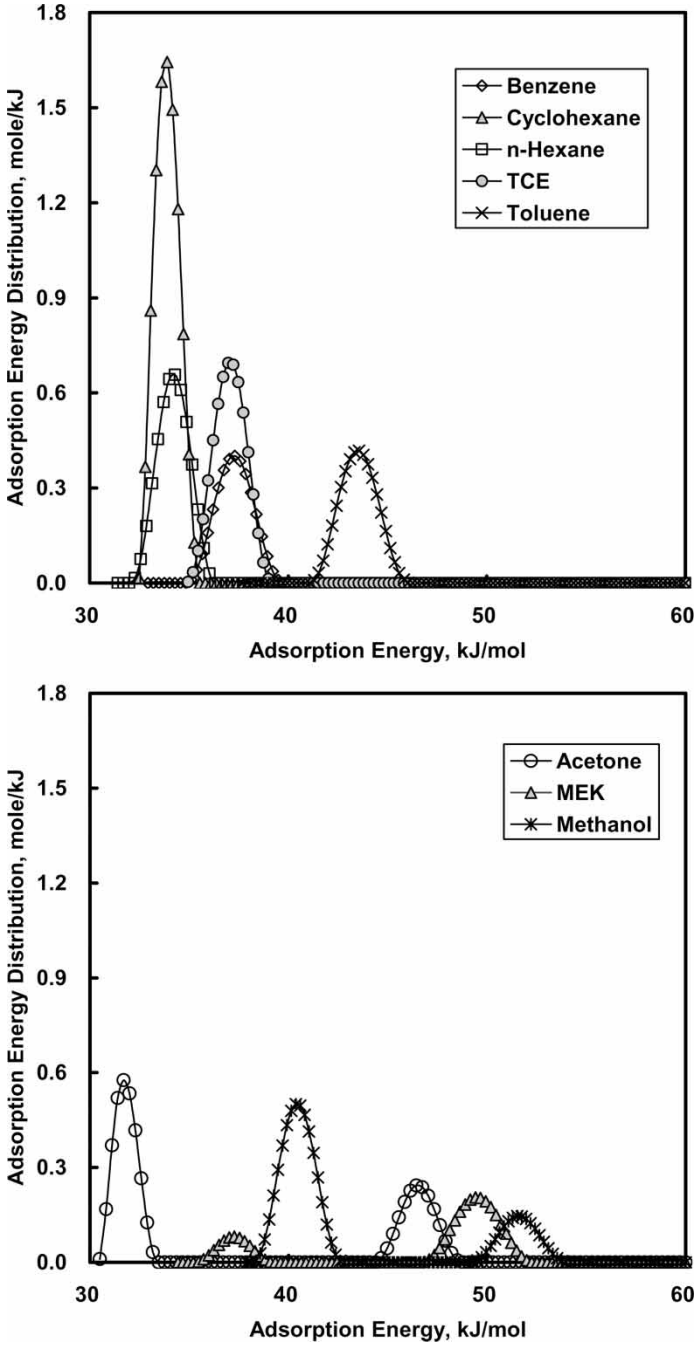

Figure 10. Adsorption energy distributions for different VOCs on MCM-48 calculated with the BET equation at 303.15 K.

the height of the energy peak has around three times larger than the first curve. In the present study, the calculated adsorption energy distribution peaks of organic adsorbates are in the range of 30–55 kJ mol^{-1}. The number of peaks of adsorption energy distribution for VOCs is highly associated with the surface heterogeneities on MCM-48. This may come from the structural differences between organic molecules (37–38), (42–43). In addition, it needs to be noted that the Debye dipole moment is closely related with the adsorption energy patterns of VOCs on MCM-48.

CONCLUSIONS

Adsorption equilibria of different organic compounds were studied to understand the surface characteristics of mesoporous media. It was found that the isosteric enthalpy of adsorption for VOCs has a close connection with the ionization potential of organic compounds. The isosteric enthalpy of adsorption varied between 37 and 49 kJ/mol with the surface loading of organic compounds. The order of magnitude for the isosteric enthalpy of adsorption of VOCs is toluene> benzene> TCE> acetone> cyclohexane> n-hexane. The obtained mobile adsorption entropy values are between 47 and 53 J K^{-1} mol^{-1}, whereas the localized values are located between 152 and 170 J K^{-1} mol^{-1}. The results of the thermodynamic properties indicated that the observed entropy change is close to mobile adsorption. MCM-48 seems to have a higher affinity to polar organic compounds than to non-polar organics according to the results of capillary condensation pressure, organophilicity, and the adsorption energy distribution of VOCs. The order of affinity to VOCs on MCM-48 is acetone > methanol > n-hexane > benzene > cyclohexane > toluene. The shape of adsorption energy distribution depends mainly on the adsorption step and the Debye dipole moment. The application of a different method can provide valuable information for the surface heterogeneity of the VOCs + MCM-48 adsorption system.

ACKNOWLEDGEMENT

This work was supported by grant No. (R-01-2001-00414-0(2003)) from the Korea Science & Engineering Foundation.

REFERENCES

1. Sing, K.S.W., Everett, D.H., Haul, R.A.W., Moscou, L., Pierotti, R.A., Rouquerol, J., and Siemieniewska, T. (1985) Reporting physisorption data for

gas/solid systems with speical reference to the determination of surface area and porosity (Recommendations 1984). *Pure Appl. Chem.*, 57 (4): 603.
2. Beck, J.S., Vartuli, J.C., Roth, W.J., Leonowicz, M.E., Kresge, C.T., Schmitt, K.D., Chu, C.T.-W., Olson, D.H., Sheppard, E.W., McCullen, S.B., Higgins, J.B., and Schlenker, J.L. (1992) A new family of mesoporous molecular sieves prepared with liquid crystal templates. *J. Am. Chem. Soc.*, 114: 10834.
3. Zhao, D.Y. and Goldfarb, D. (1995) Synthesis of mesoporous manganosilicates-MN-MCM-41, MN-MCM-48, and MN-MCM-L. *J. Chem. Soc. Chem. Commu.*, 875.
4. Ryoo, R., Jun, S., Kim, J.M., and Kim, M.J. (1997) Generalised route to the preparation of mesoporous metallosilicates via post-synthetic metal implantation. *Chem. Commun.*, 2225.
5. Hartmann, M., Racouchot, S., and Bischof, C. (1997) Synthesis and redox properties of MCM-48 containing copper and zinc. *Chem. Commun.*, 2367.
6. Kawi, S. and Te, M. (1998) MCM-48 supported chromium catalyst for trichloroethylene oxidation. *Catalysis Today*, 44: 101.
7. Froba, M., Kohn, R., Bouffaud, G., Richard, O., and van Tendeloo, G. (1999) Fe_2O_3 nanoparticles within mesoporous MCM-48 silica: In situ formation and characterization. *Chem. Mater.*, 11: 2858.
8. Hartmann, M. and Bischof, C. (1999) Mechanical stability of mesoporous molecular sieve MCM-48 studied by adsorption of benzene, *n*-heptane, and cyclohexane. *J. Phys. Chem. B*, 103: 6230.
9. Morey, M.S., Bryan, J.D., Schwarz, S., and Stucky, G.D. (2000) Pore surface functionalization of MCM-48 mesoporous silica with tungsten and molybdenum metal centers: Perspective on catalytic peroxide activation. *Chem. Mater.*, 12: 3435.
10. Zhao, X.S. and Lu, G.Q. (2001) Organophilicity of MCM-41 adsorbents studied by adsorption and temperature-programmed desorption. *Colloids and Surfaces A*, 179: 261.
11. Yuan, Z.Y., Luo, Q., Liu, J.Q., Chen, T.H., Wang, J.Z., and Li, H.X. (2001) Synthesis and characterization of boron-containing MCM-48 cubic mesoporous molecular sieves. *Microporous Mesoporous Mater.*, 42: 289.
12. Han, Y.J., Watson, J.T., Stucky, G.D., and Butler, A. (2002) Catalytic activity of mesoporous silicate-immobilized chloroperoxidase. *J. Mol. Catal. B: Enzym.*, 17: 1.
13. Lee, J.W., Lee, J.W., Shim, W.G., Suh, S.H., and Moon, H. (2003) Adsorption of chlorinated volatile organic compounds on MCM-48. *J. Chem. Eng. Data.*, 48: 381.
14. Oh, J.S., Shim, J.W., Lee, J.W., Kim, J.H., Moon, H., and Seo, G. (2003) Adsorption equilibrium of water vapor on mesoporous materials. *J. Chem. Eng. Data*, 48: 1458.
15. Schmidt, R., Stocker, M., Akporiaye, D., Torstad, E.H., and Olsen, A. (1995) High-resolution electron-microscopy and X-ray diffraction studies of MCM-48. *Microporous Materials*, 5: 1.
16. Alfredsson, V. and Anderson, M.W. (1996) Structure of MCM-48 revealed by transmission electron microscopy. *Chem. Mater.*, 8: 1141.
17. Kim, J.M., Kim, S.K., and Ryoo, R. (1998) Synthesis of MCM-48 single crystals. *Chem. Commun.*, 259.
18. Carlsson, A., Kaneda, M., Sakamoto, Y., Terasaki, O., Ryoo, R., and Joo, S.H. (1999) The structure of MCM-48 determined by electron crystallography. *J. Electron Microsc.*, 795.

19. Kruk, M. (1998) *Modelling of Gas Adsorption on Heterogeneous Porous Solids*; Ph D Thesis, Kent State University.
20. Branton, P.J., Hall, P.G., and Sing, K.S.W. (1995) Physisorption of alcohols and water vapour by MCM-41, a model mesoporous adsorbent. *Adsorption.*, 1: 77.
21. Branton, P.J., Hall, P.G., Treguer, M., and Sing, K.S.W. (1995) Adsorption of carbon-dioxide, sulfur-dioxide and water vapor by MCM-41, a model mesoporous adsorbent. *J. Chem. Soc., Faraday Trans.*, 91: 2041.
22. Ravikovitch, P.I., Wei, D., Chueh, W.T., Haller, G.L., and Neimark, A.V. (1997) Evaluation of pore structure parameters of MCM-41 catalyst supports and catalysts by means of nitrogen and argon adsorption. *J. Phys. Chem. B*, 101: 3671.
23. Morishige, K., Fujii, H., Uga, M., and Kinukawa, D. (1997) Capillary critical point of argon, nitrogen, oxygen, ethlylene, and carbon dioxide in MCM-41. *Langmuir*, 13: 3494.
24. Llewellyn, P.L., Grillet, Y., Rouquerol, J., Martin, C., and Coulomb, J.-P. (1996) Theromodynamic and structural properties of physisorbed phases within the model mesoporous adsorbent M41S (pore diameter 2.5 nm). *Surf. Sci.*, 352–354: 468.
25. Maddox, M.W., Olivier, J.P., and Gubbins, K.E. (1997) Charaterization of MCM-41 using molecular simulation: Heterogeneity effects. *Langmuir*, 13: 1737.
26. Nguyen, C., Sonwane, C.C., Bhatia, S.K., and Do, D.D. (1998) Adsorption of benzene and ethanol on MCM-41 material. *Langmuir*, 14: 4950.
27. Choudhary, V.R. and Mantri, K. (2000) Adsorption of aromatic hydrocarbons on highly siliceous MCM-41. *Langmuir*, 16: 7031.
28. Riberio Carrott, M.M.L., Candeias, A.J.E., Carrott, P.J.M., Ravikovitch, P.I., Neimark, A.V., and Sequeria, A.D. (2001) Adsorption of nitrogen, neopentane, n-hexane, benzene and methanol for the evaluation of pore sizes in silica grades of MCM-41. *Microporous Mesoporous Mater.*, 47: 323.
29. Boger, T., Roesky, R., Glaser, R., Ernst, S., Eigenberger, G., and Weitkamp, J. (1997) Influence of the aluminum content on the adsorptive properties of MCM-41. *Microporous Mater.*, 8: 79.
30. Rathousky, J., Zukal, A., Franke, O., and Schulz-Ekloff, G. (1995) Adsorption on MCM-41 mesporous molecular-sieves. 2. cyclopentane isotherms and their temperature-dependence. *J. Chem. Soc., Faraday Trans.*, 91: 937.
31. Gusev, V.Y., Feng, X., Bu, Z., Haller, G.L., and O'Brien, J.A. (1996) Mechanical stability of pure silica mesoporous MCM-41 by nitrogen adsorption and small-angle X-ray diffraction measurements. *J. Phys. Chem.*, 100: 1985.
32. Springuel-Huet, M.-A., Bonardet, J.-L., Gédéon, A., Yue, Y., Rommannikov, V.N., and Fraissard, J. (2001) Mechanical properties of mesoporous silicas and alumina-silicas MCM-41 and SBA-15 studied by N2 adsorption and Xe-129 NMR. *Microporous Mesoporous Mater.*, 44: 775.
33. Qiao, S.Z., Bhatia, S.K., and Zhao, X.S. (2003) Prediction of multilayer adsorption and capillary condensation phenomena in cylindrical mesopores. *Microporous Mesoporous Mater.*, 65: 287.
34. Brunauer, S., Emmett, P.H., and Teller, E. (1938) Adsorption of gases in multimolecular layers. *J. Am. Chem. Soc.*, 60: 309.
35. Barrett, E.P., Joyner, L.G., and Halenda, P.P. (1951) The determination of pore volume and area distributions in porous substances. I. Computations from nitrogen isotherms. *J. Am. Chem. Soc.*, 73: 373.
36. Shim, W.G., Lee, J.W., and Moon, H. (2003) Adsorption of carbon tetrachloride and chloroform on activated carbon at (300.15, 310.15, 320.15, and 330.15) K. *J. Chem. Eng. Data.*, 48: 286.

37. Lee, J.W., Shim, W.G., and Moon, H. (2004) Adsorption equilibrium and kinetics for capillary condensation of trichloroethylene on MCM-41 and MCM-48. *Microporous Mesoporous Mater.*, 73: 109.
38. Lee, J.W., Shim, W.G., Yang, M.S., and Moon, H. (2004) Adsorption isotherms of polar and nonpolar organic compounds on MCM-48. *J. Chem. Eng. Data.*, 49: 502.
39. Gressg, S.J. and Sing, S.W. (1982) *Adsorption, Surface Area and Porosity*; Academic Press: New York.
40. Suzuk, M. (1990) *Adsorption Engineering*; Kodansha: Tokyo.
41. Reid, R.C., Prausnitz, J.M., and Poling, B.E. (1987) *The Properties of Gases & Liquids*; McGraw-Hill Company: Tokyo.
42. Jaroniec, M. and Madey, R. (1988) *Physical Adsorption on Heterogeneous Solids*; Elsevier: Amsterdam.
43. Rudzinski, W. and Everett, D. (1991) *Adsorption of Gases on Heterogeneous Solid Surfaces*; Academic Press: London.
44. Roginsky, S.S. (1948) *Adsorption and Catalysis on Heterogeneous Solid Surfaces*; Academiy of Sciences of U.S.S.R: Moscow.
45. Kalantzopoulou, F.R. (2004) Determination of isotherms by gas-solid chromatography applications. *J. Chromato. A.*, 1037: 191.
46. Weese, J. (1992) A reliable and fast method for the solution of Fredholm integral equations of the first kind based on Tikhonov regularization. *Comput. Phys. Commun.*, 69: 99.
47. Roth, T., Marth, M., Weese, J., and Honerkamp, J. (2001) A generalized regularization method for nonlinear ill-posed problems enhanced for nonlinear regularization terms. *Comput. Phys. Commun.*, 139: 279.
48. Brauer, P., Fassler, M., and Jaroniec, M. (1985) Numerical solutions of the adsorption integral equation utilizing the spline functions. *Thin Solid Films*, 123: 245.
49. Szombathely, M.V., Brauer, P., and Jaroniec, M. (1992) The solution of adsorption integral equations by means of the regularization method. *J. Comput. Chem.*, 13: 17.
50. Puziy, A.M., Matynia, T., Gawdzik, B., and Poddubnaya, O.I. (1999) Use of CONTIN for calculation of adsorption energy distribution. *Langmuir*, 15: 6016.
51. Gun'ko, V.M., Ledoba, R., Turov, V.V., Villieras, F., Skubiszewska-zieba, J., Chodorowski, S., and Marciniak, M. (2001) Structural and energetic nonuniformities of pyrocarbon-mineral adsorbents. *J. Colloid Interface Sci.*, 238: 340.
52. Brunauer, S., Deming, L.S., Deming, E., and Teller, E. (1940) On a theory of van der Waals adsorption of gases. *J. Am. Chem. Soc.*, 62: 1723.
53. Qiao, S.Z., Bhatia, S.K., and Nicholson, D. (2004) Study of hexane adsorption in nanoporous MCM-41 silica. *Langmuir*, 20: 389.
54. Tanchoux, N., Trens, P., Maldonado, D., Renzeo, F.D., and Fajula, F. (2004) The adsorption of hexane over MCM-41 type materials. *Colloids and Surfaces A: Physicochem. Eng. Aspects*, 246: 1.
55. Janchen, J., Stach, H., Busio, M., and van Wolput, J.H.M.C. (1998) Microcalorimetric and spectroscopics studies of the acidic- and physisorption characteristics of MCM-41 and zeolites. *Thermochimica Acta*, 321: 33.